SCIENTIFIC REPORTS

OPEN

SUBJECT AREAS:
BIOMEDICAL ENGINEERING
PRE-CLINICAL STUDIES

Received
24 April 2014

Accepted
26 June 2014

Published
14 July 2014

Correspondence and requests for materials should be addressed to P.C.L. (paichi@ntu.edu.tw)

Synergistic delivery of gold nanorods using multifunctional microbubbles for enhanced plasmonic photothermal therapy

Yu-Hsin Wang[1], Shi-Ping Chen[1], Ai-Ho Liao[2], Ya-Chuen Yang[3], Cheng-Ru Lee[3], Cheng-Han Wu[4], Pei-Chun Wu[4], Tzu-Ming Liu[4], Churng-Ren Chris Wang[3] & Pai-Chi Li[1,5]

[1]Graduate Institute of Biomedical Electronics and Bioinformatics, National Taiwan University, Taipei, Taiwan, [2]Graduate Institute of Biomedical Engineering, National Taiwan University of Science and Technology, Taipei, Taiwan, [3]Department of Chemistry and Biochemistry, National Chung-Cheng University, Chia-Yi, Taiwan, [4]Graduate Institute of Biomedical Engineering, National Taiwan University, Taipei, Taiwan, [5]Department of Electrical Engineering, National Taiwan University, Taipei, Taiwan.

Plasmonic photothermal therapy (PPTT) using plasmonic nanoparticles as efficient photoabsorbing agents has been proposed previously. One critical step in PPTT is to effectively deliver gold nanoparticles into the cells. This study demonstrates that the delivery of gold nanorods (AuNRs) can be greatly enhanced by combining the following three mechanisms: AuNRs encapsulated in protein-shell microbubbles (AuMBs), molecular targeting, and sonoporation employing acoustic cavitation of microbubbles (MBs). Both *in vitro* and *in vivo* tests were performed. For molecular targeting, the AuMBs were modified with anti-VEGFR2. Once bound to the angiogenesis markers, the MBs were destroyed by ultrasound to release the AuNRs and the release was confirmed by photoacoustic measurements. Additionally, acoustic cavitation was induced during MB destruction for sonoporation (i.e., increase in transient cellular permeability). The measured inertial cavitation dose was positively correlated with the temperature increase at the tumor site. The quantity of AuNRs delivered into the cells was also determined by measuring the mass spectrometry and observed using third-harmonic-generation microscopy and two-photon fluorescence microscopy. A temperature increase of 20°C was achieved *in vitro*. The PPTT results *in vivo* also demonstrated that the temperature increase (>45°C) provided a sufficiently high degree of hyperthermia. Therefore, synergistic delivery of AuNRs was demonstrated.

Recent advancements in biotechnology and nanotechnology have allowed the integration of molecular imaging and targeted therapy, also known as theranosis[1]. Molecular imaging involves the visualization of a specific molecular process, and it can be used to study disease progression or to monitor a therapeutic process[2]. A micron- or nanometer-sized molecular probe typically needs to be designed and utilized. Such a probe not only serves as a contrast agent for imaging, it also provides targeting capabilities at the molecular level. For example, radioactive isotopes have been used for positron-emission tomography and single-photon-emission computed tomography[3]. In addition to imaging, these probes can be used to deliver drugs or therapeutic agents[1]. Multimodality molecular probes have also been developed to exploit the synergy between different imaging and therapeutic mechanisms[4–9]. We previously reported on a dual-modality contrast agent comprising gold nanorods (AuNRs) encapsulated in protein-shell microbubbles (AuMBs) for use in ultrasound and photoacoustic (PA) imaging and provided characterizations of AuMBs, such as optical absorption and size distribtuion[10]. The multimodality agent has the potential to combine benefits from different modalities, and also to allow anatomical, functional, and molecular imaging to be performed simultaneously. Our proposed AuMBs have protein-shell microbubbles (MBs) and are used as an agent for both PA molecular imaging and targeted plasmonic photothermal therapy (PPTT)[11]. The aspect ratio of the AuNRs can be varied from low to high in order to tune their peak optical absorption wavelength. A near-infrared wavelength is typically used to ensure the adequate penetration of light into the tissue. Since the AuNRs efficiently produce both thermal and PA responses, they have been widely investigated for both PA imaging and PPTT[12,13].

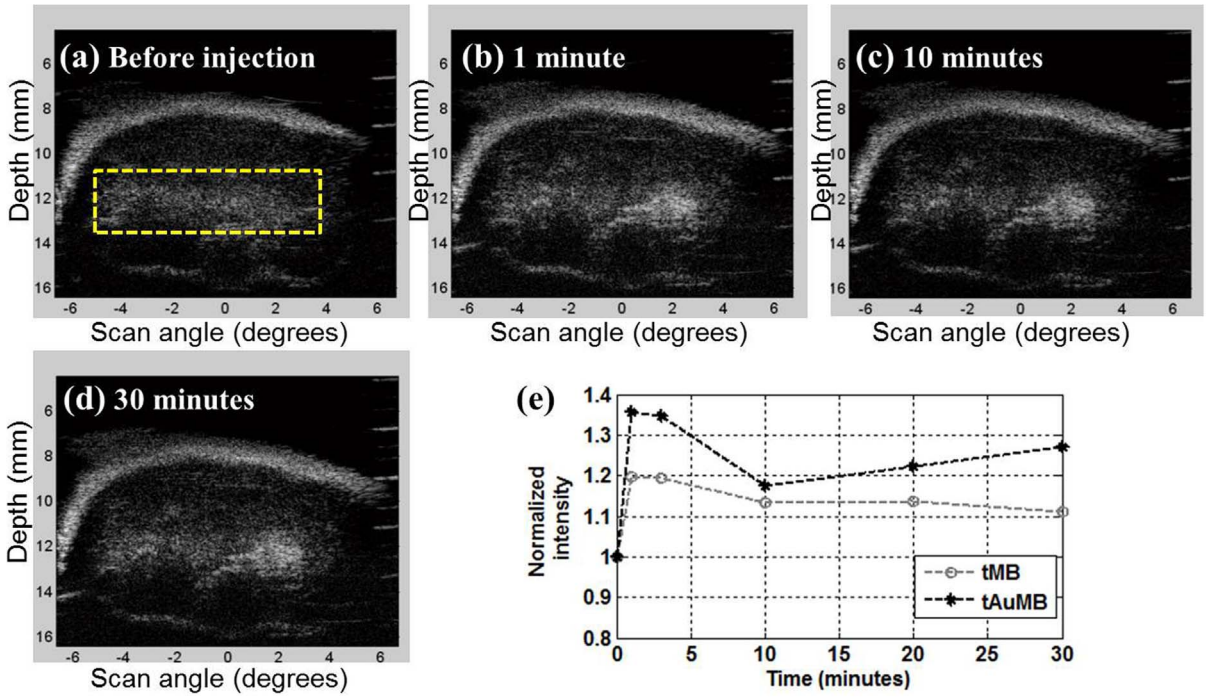

Figure 1 | Ultrasound molecular images obtained when tAuMBs were injected into the mouse. Tumor B-mode images were obtained (a) before the injection and at (b) 1 minute, (c) 10 minutes, and (d) 30 minutes after the injection. (e). Time–intensity curves calculated for the intensity within the region of interest (rectangular box in panel a) in the B-mode images for the tMB and tAuMB cases.

Combining AuNRs with MBs has the potential to improve their delivery efficiency in several different ways. First, gas-filled echogenic MBs, which have been used as the ultrasound contrast agent in clinical applications, can also be used as targeting drug-delivery vehicles[14]. The relative large size of MBs (typically 1–3 microns in diameter) restricts their extravasation, so they are used mostly for identifying intravascular markers, such as in the recognition of angiogenesis in cancerous lesions[15]. However, the delivery of AuNRs can be enhanced by active targeting with antibody bioconjugation on the surface of AuMBs. Moreover, the use of molecular binding extends the retention period of these targeted AuMBs in the tumor relative to using plain MBs (i.e., without bioconjugation). MB accumulation can be observed using ultrasound imaging (i.e., ultrasound molecular imaging)[16].

Second, the encapsulated AuNRs need to be released from the AuMBs once they reach the target site. This can be achieved by applying ultrasound to destroy the AuMBs. The cavitation effects that occur during the destruction process temporarily increase cell permeability, which can have the additional beneficial effect of enhancing the delivery of AuNRs into the cells. This is also known as sonoporation[17]. Enhanced cavitation can be anticipated with the presence of MBs compared to the ultrasound alone because the MBs act as cavitation nuclei. When acoustic stimulation induces MB destruction, both vascular permeability and cellular uptake are enhanced. It has been reported that cavitating MBs can assist drug release, promote therapy efficacy, and enhance ultrasound-induced cell death[18,19]. Previous studies have shown that the magnitudes of the expansion, contraction, and collapse of gas MBs in inertial cavitation are related to the efficacy of sonoporation and cell viability. The inertial cavitation dose can also be calculated from quantitative measurements of the energy of the broadband acoustic signal produced during cavitation[17].

The main hypothesis tested in this study is that delivery of AuNRs into tumor cells can be enhanced by combining MB encapsulation, molecular targeting, and acoustic cavitation. An enhanced cellular uptake of AuNRs will also enhance the photothermal effects. This hypothesis was tested by performing both *in vitro* and *in vivo* studies. The paper is organized as follows: Ultrasound molecular imaging was first performed to demonstrate the targeting capabilities of AuMBs. Ultrasound-assisted delivery of AuNRs is subsequently demonstrated by reporting the results of *in vitro* and *in vivo* experiments. We then examined the cellular uptake of AuNRs and related it to the inertial cavitation dose. A multimodal optical microscope was applied to investigate the improved delivery in the cells. The microscope used a Cr:forsterite femtosecond-pulse laser operating at 1230 nm to image the AuNRs based on the multiphoton absorption and the emitted fluorescence[20,21]. The morphology was investigated *in situ* with a third-harmonic-generation (THG) microscope. The paper ends with a discussion about the validity of the hypothesis.

Results

Ultrasound molecular imaging of angiogenesis targeting. CT26 colon cancer cells were injected subcutaneously into the back of 5-week-old female BALB/c mice. MBs were injected into the tail vein while imaging the mouse. Nontargeting MBs were cleared by the bloodstream very quickly (typically within 5–10 minutes)[16]. Targeting MBs (tMBs), on the other hand, bind to the specific angiogenesis marker and thus stay at the tumor site over a longer period of time. Fig. 1 shows *in vivo* images obtained in molecular imaging with targeting AuMBs (tAuMBs) using a commercial high-frequency ultrasound system operating at 40 MHz (Prospect, S-Sharp, New Taipei City, Taiwan). These tAuMBs are modified by anti-VEGFR2 being attached to the shell and thus are expected to recognize the angiogenesis marker and to extend the retention time of the tAuMBs in the tumor region. Postinjection images were collected for 30 minutes. Fig. 1a–d are tumor images obtained before the injection and at 1, 10, and 30 minutes after the injection, respectively. The average intensities are shown as a time–intensity curve in Fig. 1e. Note that the intensity is normalized to the initial value and only the region of interest (rectangular box in panel a) is considered because diffused MBs do not contribute to sonoporation. Another example, in which tMBs were injected but

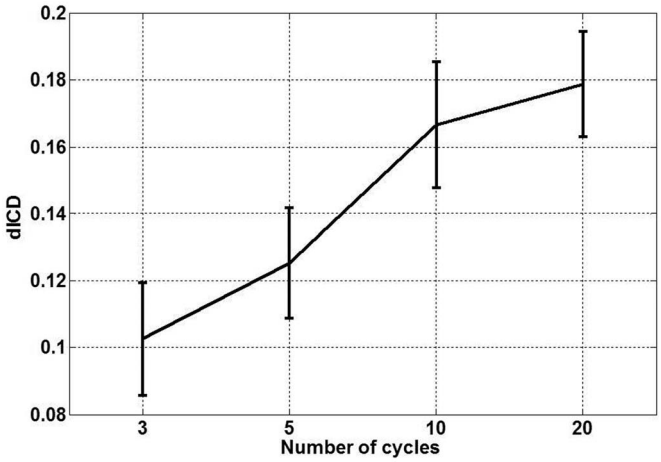

Figure 2 | Cavitation measurement results at different transmit cycles. Data are mean and SD values.

the AuNRs were not encapsulated, is also shown in Fig. 1e for comparison; in both cases the intensity was highest at 1 minute after the injection, with relative enhancements of 19.8% and 35.7% for the two cases. The enhanced intensity remained in the tumor region for more than 30 minutes after the injection, at which time the relative enhancements were 11.2% and 27.2% without and with AuNRs encapsulation, respectively. For the case with injection of non-targeted MBs, the relative enhancement in ultrasound images reached its peak within half minute and faded out within five minutes in our experiments. These results confirm the targeting ability of tAuMBs, and that they remain in the tumor vasculature for sufficiently long to allow subsequent sonoporation.

***In vitro* sonoporation experiments.** The differential inertial cavitation dose (dICD), which was previously shown to be an effective tool for detecting and analyzing inertial cavitation[17], was measured and correlated with the thermal treatment results. A 1-MHz transducer was used to generate the ultrasound stimuli that induced cavitation from MBs, while a 10-MHz transducer was used to detect the broadband signal enhancement during cavitation. The signal received by the 10-MHz transducer was converted into the root-mean-square (RMS) value in the time domain and integrated over time. Finally, the background time–amplitude curve (the measured RMS amplitude for water only) was subtracted, and the resulting amplitude—which is referred to as dICD—was used in subsequent signal analysis.

Fig. 2 shows the cavitation results with different transmit waveforms. The dICD value increases with the number of waveform cycles. As dICD increases with the pulse length, enhanced sonoporation effects are also expected.

Fig. 3 shows PA measurement results demonstrating the ultrasound-induced release of AuNRs from AuMBs. MDA-MB-231 human breast cancer cells were used. A photograph of the fixed samples with AuMBs (with and without ultrasound stimulation) and the corresponding PA image are shown in Fig. 3a. A darker region is evident on the right in the top panel, indicating AuNR uptake into the cells after the cells and AuMBs stimulated 15 times with 20 cycles of ultrasound. This is because AuNRs have deep purple color, the color of the cells also become darker after the intake of the AuNRs. The PA image in the lower panel of Fig. 3a also indicates that ultrasound can be used to release AuNRs contained within AuMBs, since the PA signal amplitude is larger for the image on the right (with controlled release) than for the image on the left (without controlled release). The results demonstrate the enhanced delivery of AuNRs associated with acoustic cavitation.

The quantity of AuNRs released is also related to the number of cycles of ultrasound stimulation. Fig. 3b shows the integrated PA signal amplitude after normalization, indicating that the PA signal increases with dICD (i.e., a longer transmit signal).

These results indicate that acoustic cavitation can be used as a controlled release method to deliver AuNRs into the cells.

The results for the efficiency of using AuMBs to deliver AuNRs into cells are shown in Fig. 4, which was measured by inductively coupled plasma mass spectrometry (ICP-MS). The ICP-MS result shows that the cells incubated with AuMBs take up slightly lower amount of AuNRs than that of those with free AuNPs. Nonetheless, the gold levels in these two control groups are very close. More importantly, significant enhancements using tAuMBs and sonoporation are demonstrated. The AuNR delivery was positively correlated with dICD.

Fig. 5 shows the temperatures recorded in the *in vitro* photothermal experiments. The samples were heated for 4 minutes with an 808-nm continuous-wave (CW) diode laser (ONSET Electro-optics, Taipei, Taiwan) at a power of 2 W/cm^2. Again, an enhanced photothermal effect was evident as dICD increased. The temperature increases were 14.6°C and 14.9°C for cells treated with AuMBs (no sonoporation) and for the cells treated with AuNRs (no MBs and no sonoporation), respectively. After ten repetitions of ultrasound stimulation, the temperature increases were 16.7°C, 21.8°C, 31.7°C, and 33.7°C in the 3-, 5-, 10-, and 20-cycle groups, respectively.

Table 1 summarizes the dICD values, the quantity of AuNR delivered into the cells, and the temperature increase. The table indicates that the AuMBs stimulated with 20 cycles of ultrasound had the largest temperature increase, quantity of AuNR, and dICD. These results are consistent with our hypothesis that sonoporation assists AuNR delivery. Moreover, the temperature increase is larger as dICD increases.

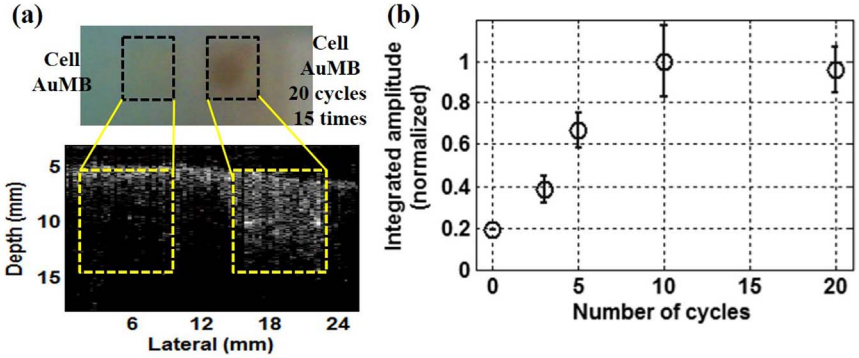

Figure 3 | Results of PA experiments (triplicate measurements). (a) Photograph of samples with and without acoustic cavitation and the corresponding PA image. (b) The measured PA signal amplitude as a function of the number of cycles of the transmit signal.

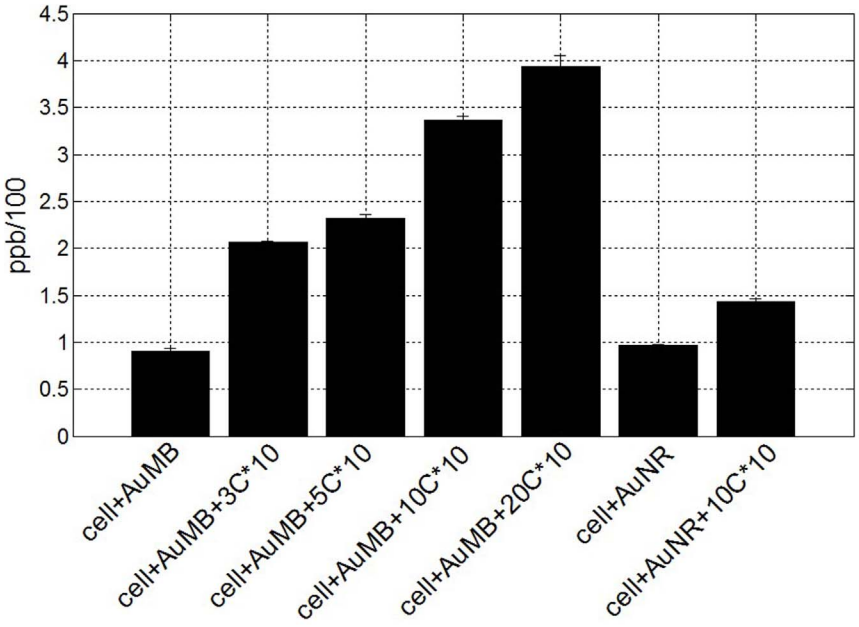

Figure 4 | **AuNR delivery under various conditions (triplicate measurements).** *n*C, number of cycles; **n*, number of experiments.

Optical observation of the AuNR distribution. Fig. 6 shows optical-microscopy images of the cell samples with AuMBs. Fig. 6a and b were obtained without ultrasound stimulation, and Fig. 6c and d were obtained with ultrasound stimulation. In this case, sonoporation was performed with 10 cycles of ultrasound applied 10 times. The THG signal shows cell morphology (appearing magenta in the figure), whereas the two-photon fluorescence (2PF) is produced mainly by AuNRs (green). It is evident that the fluorescence becomes much stronger with sonoporation, which is due to the cellular uptake of AuNRs.

***In vivo* examination with acoustic cavitation.** Sonoporation was also applied *in vivo* and nonlinear optical microscopy was used to image the distribution of AuNRs. C57BL/6-C2^J mice were used with a B16-F10 tumor model. Fig. 7 shows nonlinear optical-microscopy images of mouse ears obtained with and without injecting AuMBs into the tail vein. The 2PF signal is shown in green and the THG signal is shown in magenta. Fig. 7a and b are the observations before AuMB injection. Note that there is hardly any fluorescence in the field of view except for that from the sebaceous gland. After the injection and the application of ultrasound for sonoporation, Fig. 7c and d show the images obtained from a normal mouse and Fig. 7e and f are the images of a mouse tumor, all at the same laser power as used in the control group. The green spots in 2PF images (Figs. 7d and 7f), not along with sebaceous gland, indicate the deposition of AuMBs or their fragments. These bright spots can be further confirmed by repetitive laser heating which induces the bubble expansion.

PPTT. The enhanced PPTT with ultrasound-assisted delivery of AuNRs was also demonstrated *in vivo*. Five-week-old female NOD-SCID mice with MDA-MB-231 cells were used. Fig. 8a shows the temperatures recorded over 150 seconds for stimulation by the CW laser at an output power of 2.3 W/cm^2. The black and gray lines are the measurements of AuMB-injected groups with and without sonoporation, respectively. The region without the sonoporation was outside the tumor. The solid and dotted lines represent data from two different mice. It is found that the greater temperature increase in those cases with injected-AuMBs and sonoporation (>45°C) produced a sufficiently high degree of hyperthermia. On the other hand, those without sonoporation exhibited only minor thermal effects under the heating condition. Fig. 8b and c show photographs of the same mouse that were taken immediately after PPTT and 1 week later, respectively. Note that the same thermal dose was administered to the two regions indicated by red squares. The yellow circles indicate the tumor stimulated with ultrasound but not the CW laser. Even though the thermal dosage in current protocol may not be enough to destroy the tumor cells completely and the injected amount of AuNRs may need further optimization, it is evident that the application of sonoporation with the photothermal treatment swelled the tumor, with a scar forming several days later, while the other two regions did not exhibit noticeable changes. This indicates that tissue necrosis is induced by PPTT and is enhanced by sonoporation.

Discussion

Our previous study introduced AuMBs as a PA/ultrasound dual-modality contrast agent for imaging[10]. The present study has demonstrated that AuMBs can be used for both molecular imaging and targeted therapy (i.e., theranosis). Fig. 9 shows a schematic of the procedures involved in the proposed approach. The use of tAuMBs

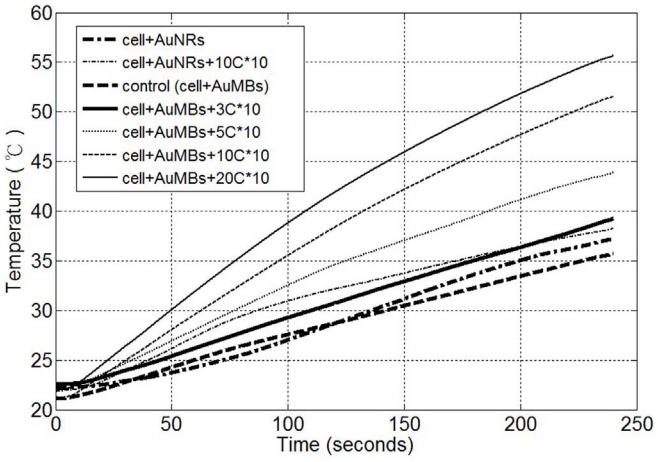

Figure 5 | **Temperature increases induced by CW laser heating in *in vitro* experiments.**

Table 1 | dICD value, quantity of AuNRs delivered into the cells, and temperature increase

Sample	Cell + AuNRs	Cell + AuMBs	Cell + AuMBs	Cell + AuMBs	Cell + AuMBs	Cell + AuMBs
Cycles × no. of experiments	0 × 0	0 × 0	3 × 10	5 × 10	10 × 10	20 × 10
dICD (V-seconds)	X	X	0.1026	0.1252	0.1665	0.1787
AuNRs in cells (ppb/100)	0.96	0.9	2.07	2.31	3.36	3.94
Temperature change (°C)	14.9	14.6	16.7	21.8	31.7	33.7

with encapsulation, active targeting, and sonoporation can enhance the delivery of AuNRs. Ultrasound molecular imaging, dICD measurements, measurements of the quantity of AuNRs delivered into the cells, PA imaging, nonlinear optical microscopy, and PPTT using a CW laser were performed to test this hypothesis in both cell models and mice.

Ultrasound molecular imaging confirmed the active targeting of the tAuMBs in the tumor. The cavitation induced by a time-varying acoustic field disrupted the AuMBs and resulted in increased transient cellular permeability (i.e., sonoporation). The quantity of AuNRs delivered was proportional to the number of cycles of the ultrasound stimulus. The PA increase with ten repetitions of sonoporation was much higher when using AuMBs than in the control group. In addition, the temperature was increased by more than 20°C in the photothermal experiments. The enhanced 2PF signals of the treated cells, which were produced by uptake of the AuNRs, were also observed in nonlinear optic microscopy. These observations provide strong evidence that ultrasound-induced MB disruption assists the cellular delivery of AuNRs. Therefore, we can conclude that the controlled release is feasible and can further enhance the therapeutic effects.

Methods

Preparation of (non)targeted AuMBs. AuMBs were prepared as described for our previous study[10]. The targeting modification is based on the avidin-biotin system. Specifically, avidin was added for synthesis and incorporated into the albumin shell. The avidin-AuMBs were prepared by sonicating a solution containing 2.8 nM AuNRs, 2% human serum albumin (HSA, Octapharma, Vienna, Austria), 0.04% (w/v) avidin, and perfluorocarbon (C_3F_8) gas. The absorption peak of an AuNR is around 800 nm. Note that the HSA and AuNRs were mixed overnight before sonication, after which the AuMBs were washed three times to remove free avidin. Biotinylated antimouse VEGFR2 (eBioscience, San Diego, CA) was added (40 μg) and incubated with avidin-incorporated AuMBs for at least 30 minutes at 4°C. Two washes were then performed to remove unbound antibodies. For *in vitro* studies, nontargeted AuMBs were prepared by sonicating the HSA-AuNR mixture. No avidin or antibody was added during preparation.

Ultrasound molecular imaging. To examine the targeting efficacy in the tumor, approximately 2×10^6 CT26 colon cancer cells were injected subcutaneously into the dorsal side of 5-week-old female BALB/c mice using a 28-gauge needle[22]. All animal experiments were performed using an animal care protocol approved by the National Animal Center of Taiwan. All mice were maintained according to the regulations of National Taiwan University Hospital. The mice were purchased from Animal Center of National Taiwan University Hospital. About 2 weeks later, a high-frequency ultrasound system (Prospect, S-Sharp, New Taipei City, Taiwan) was used to acquire B-mode images with a 40-MHz transducer, which had a diameter of 6 mm and a fixed focus at 12 mm. The tumor-bearing mice were anesthetized with 2% isoflurane in oxygen applied at a flow rate of 2 L/min. After identifying the tumor, about 150 μL of anti-VEGFR2 AuMBs was injected into the lateral tail vein. These images were recorded for 30 minutes to confirm the accumulation and extended retention period of tMBs.

***In vitro* tests of enhanced delivery of AuNRs with acoustic cavitation.** The *in vitro* tests were performed with MDA-MB-231 human breast cancer cells that were purchased from the ATCC and grown with IL-15 medium in a closed T-75 flask. After 3 days of growth, tumor cells were harvested with the aid of 0.25% trypsin and 0.02% EDTA, and resuspended in phosphate-buffered saline. Each vial contained 3×10^6 cells and around 5×10^8 AuMBs in a 1.8-mL solution (about 4×10^6 cells in the photothermal experiment). Samples in the AuNR groups contained the same number of cells, and the concentration of the AuNR solution was around 0.28 nM for each vial; this was equivalent to the amount in the original (HSA-AuNR mixture) solution. In each batch of experiments, the sample vial was placed in a 2% agarose phantom at the focal position of the transducer (i.e., 4.9 cm from the transducer). Acoustic cavitation was induced by a 1-MHz transducer (V302, Panametrics-NDT, Waltham, MA), with the transmitted waveforms generated by a digital-to-analog converter (CompuGen 1100, GaGe, Lockport, IL) and amplified by a power amplifier (250A250A, Amplifier Research, Souderton, PA). The cavitation experiments employed 1-MHz pulsed sinusoids at a repetition frequency of 100 Hz and acoustic pressures of about 1.82 MPa. The inertial cavitation dose was varied by using sinusoids with 3, 5, 10, or 20 cycles[17]. A 10-MHz transducer (V312, Panametrics-NDT) was used for detection, with the signal being sent to a preamplifier (5077PR, Panametrics). Each sample was stimulated at least ten times with ultrasound for 1 minute and intermittently shaken mildly by hand in order to homogenize the sample. After ultrasound stimulation, the cells were washed and collected by two 1000-rpm centrifugations and natural precipitation.

ICP-MS was used for gold quantification. The collected cells were digested using 2 ml of aqua regia at 75–85°C for 5 hours. 100 μL of concentrated samples was then diluted to 10 mL with 2% HCl. A series of gold standard solutions (18 14, 10, 6, 2, and 0 ppb) were prepared and diluted with 2% HCl before each experiment. The resulting calibration curve was used to determine the cellular uptake amount of gold.

PA phantom imaging and photothermal experiments. In the PA experiments, the collected cells were fixed by 1% agarose in a volume of 0.5 ml and embedded into an agarose base for examination. The samples were irradiated by a Ti:sapphire laser (CF-125, SOLAR TII, Minsk, Belarus) that used an Nd:YAG laser as the pump (LS-2137 U, LOTIS TII, Minsk, Belarus). A custom-made 20-MHz fiber-integrated transducer was used for detection, with the PA signal being sent to a preamplifier (5077PR, Panametrics). The transducer was mounted on a precision translation stage (HR8, Nanomotion, Yokneam, Israel) to obtain a B-scan image or to visualize a particular region of interest. These signals were recorded by a data acquisition card (CompuScope 14200, GaGe, Lockport, IL) at 100 M samples/seconds. All PA experiments were performed at an energy level of around 6 mJ/cm^2 per pulse. For comparisons, the amplitude values of the acquired signals around the center of the sample region were summed. For photothermal experiments, the 808-nm CW diode laser was used to heat the 0.5-mL samples at a power of 2.5 W/cm^2. Those samples were directly loaded in Eppendorf tubes without agarose fixation. The temperature increase was recorded by an infrared thermometer (thermoMETER LS, Optris, Berlin, Germany).

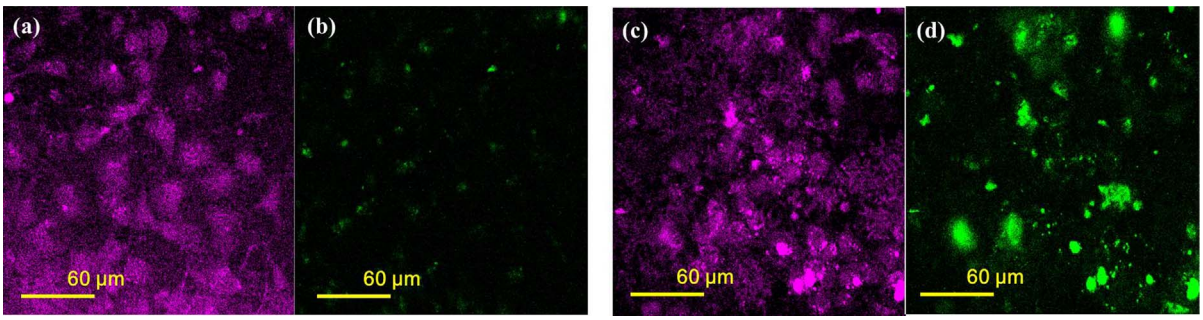

Figure 6 | Nonlinear optical microscopy with ((a) and (b)) and without ((c) and (d)) sonoporation. The THG signal appears magenta in panels (a) and (c), while the 2PF signal appears green in panels (b) and (d).

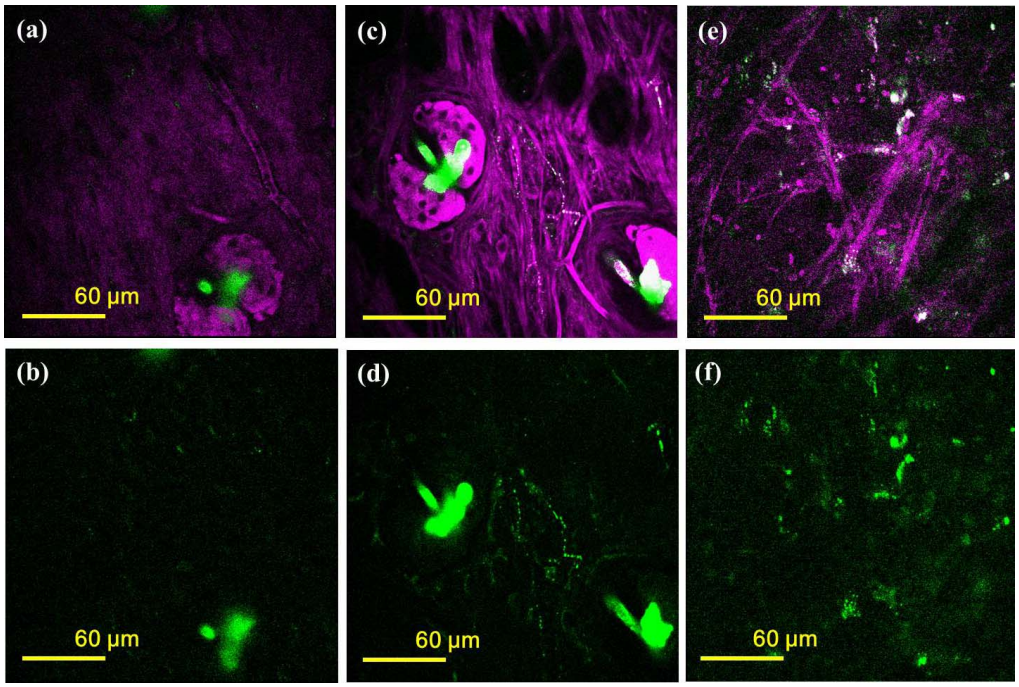

Figure 7 | Nonlinear optical microscopy of the mouse ears (magenta: THG, green: 2PF). Panels (a) and (b) are THG-2PF and 2PF-only images of a reference without AuMB injection, respectively. Images of a normal mouse ear after the injection and sonoporation are shown in panels (c) and (d), while panels (e) and (f) are images for a mouse tumor.

Observation with nonlinear optical microscopy. The collected cells in some of the groups were used for nonlinear optical observations. Samples that had either been stimulated or not stimulated with AuMB-assisted sonoporation were loaded into glass-bottom petri dishes with medium. After overnight incubation, the samples were placed on the platform of an inverted optical microscope (IX71, Olympus, Tokyo Japan). The microscope was used to acquire 2PF (>650 nm) and THG signals excited by the Cr:forsterite femtosecond-pulse laser. The laser beam is scanned in two dimensions by a galvanometer and tightly focused with a water-immersion objective (NA = 1.2, 60×, Olympus). The output power at the objective was around 70 mW in the cell study. Software (FluoView 300, Olympus) was used to reconstruct images of size 512 by 512 pixels from the signals amplified by photomultiplier tubes (R928, Hamamatsu, Hamamatsu City, Shizuoka, Japan).

***In vivo* enhanced delivery of AuNRs with acoustic cavitation.** The enhanced delivery of AuNRs was demonstrated in tumor-bearing mice. For *in vivo* PPTT, the AuNR concentration was increased 3.5-fold relative to than used in *in vitro* examinations; that is, the AuNR concentration was around 10 nM in the HSA-AuNR solution (before sonication) to prepare the AuMBs.

In vivo delivery was first examined with the aid of an optical microscope. In the experiments, the animal model was C57BL/6-C2^{J} mice and the tumor model was B16-F10, purchased from ATCC. Melanoma cells were incubated with Dulbecco's modified Eagle's medium plus 13% fetal bovine serum and grown in a humidified atmosphere containing 5% CO_2 at a constant temperature of 37°C. Both a healthy mouse and a tumor-bearing mouse were examined. To implant a tumor, 1.5×10^6 B16-F10 cells were injected subcutaneously into the ear of the mouse at an age of 4 weeks. When the width of the tumor reached 5 mm, the mouse was anesthetized intraperitoneally with Avertin and its ear was immobilized and imaged with the aid of the optical microscope. The output power at the objective was approximately 150 mW for *in vivo* studies, and no fluorescence signals were detected around the vessels prior to sonoporation. tAuMBs (200 μL) were then injected intravenously into the tail vein of the mouse at a concentration of 6.8×10^8/mL. Five minutes later the mouse was removed from the stage and positioned for sonoporation. The acoustic parameters were similar to those in the *in vitro* tests except that a stronger acoustic field (20 cycles, 2.98 MPa) was applied to the lesion. For acoustic coupling, an agarose cylinder with a height of 4.9 cm and coupling gel were placed between the tumor and the transducer. The sonoporation procedure was performed for 5 minutes, and the mouse was then again immobilized on the stage for another microscopy examination.

The MDA-MB-231 tumor model was used in the photothermal experiments. The tumor cells were incubated as described above. After harvesting the cells, 0.1 mL of the cell suspension (containing 5×10^6 tumor cells) was injected subcutaneously into the dorsal side of a 5-week-old female nod-SCID mouse. All mice were maintained according to the regulations of National Taiwan University Hospital. Most of the tumors had grown to 100 mm^3 at 2 weeks after inoculation. During the experiments, the mice were kept anesthetized with 2% isoflurane in oxygen at 2 L/minute and its skin hair was gently removed with cream. Anti-VEGFR2 AuMBs in a volume of 300 μL (at a concentration of 9×10^8/mL) were injected intravenously into the tail

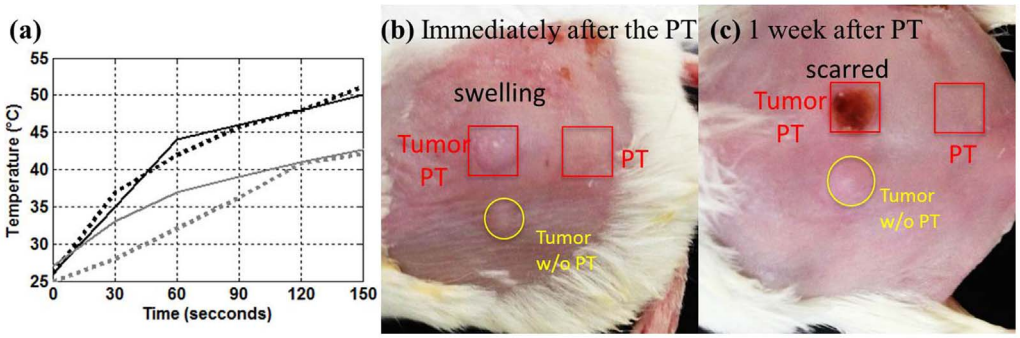

Figure 8 | Demonstration of enhanced PPTT. Panel (a) shows the temperatures induced during CW laser heating. Black and gray lines are measurements in sonoporation and nonsonoporation regions, respectively. Panels (b) and (c) are photographs of the mouse tumors taken immediately after the treatment and 1 week later, respectively.

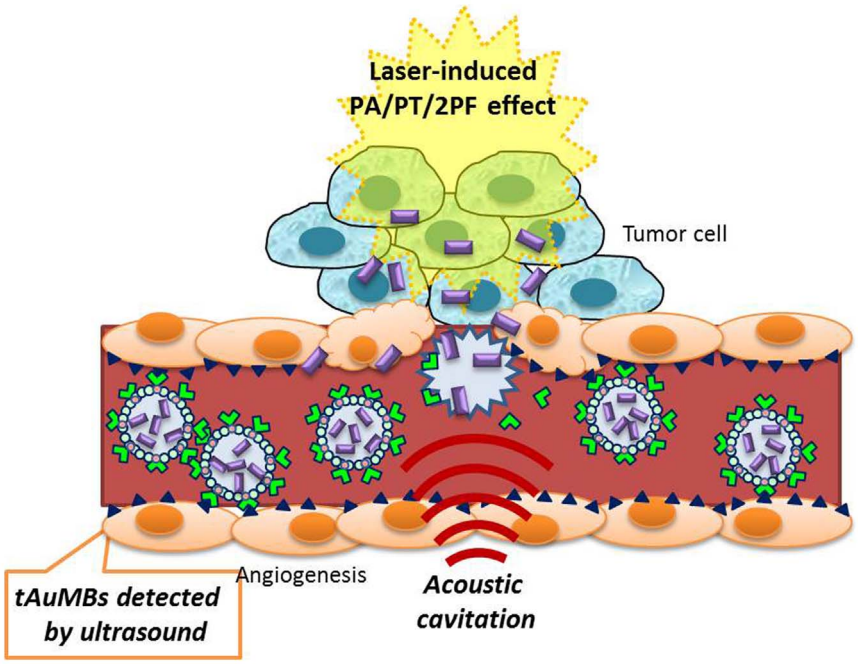

Figure 9 | Schematic summarizing the following mechanisms revealed in this study: the active targeting of tAuMBs in angiogenesis, acoustic cavitation to increase permeability, and enhanced photon-related effects (e.g., PA, photothermal, and multiphoton fluorescence).

vein of the mouse. Sonoporation was then applied to the tumor for 5 minutes with the aid of acoustic coupling gel. After sonoporation the gel was removed and the 808-nm CW diode laser was turned on to heat the lesion for 3 minutes. The temperature of the lesion was simultaneously recorded by an infrared thermometer (thermoMETER LS, Optris) every 30 seconds.

1. Kim, K. *et al.* Tumor-homing multifunctional nanoparticles for cancer theragnosis: Simultaneous diagnosis, drug delivery, and therapeutic monitoring. *J. Control. Release* **146**, 219–227 (2010).
2. Pysz, M. A., Gambhir, S. S. & Willmann, J. K. Molecular imaging: current status and emerging strategies. *Clin. Radiol.* **65**, 500–516 (2010).
3. Khalil, M. M., Tremoleda, J. L., Bayomy, T. B. & Gsell, W. Molecular SPECT imaging: an overview. *Int. J. Mol. Imaging* **2011**, 796025 (2011).
4. Koo, Y. E. *et al.* Brain cancer diagnosis and therapy with nanoplatforms. *Adv. Drug. Deliv. Rev.* **58**, 1556–1577 (2006).
5. Kobayashi, H., Longmire, M. R., Ogawa, M., Choyke, P. L. & Kawamoto, S. Multiplexed imaging in cancer diagnosis: applications and future advances. *Lancet Oncol.* **11**, 589–595 (2010).
6. Ko, H. Y., Choi, K. J., Lee, C. H. & Kim, S. A multimodal nanoparticle-based cancer imaging probe simultaneously targeting nucleolin, integrin $\alpha_v\beta_3$ and tenascin-C proteins. *Biomaterials* **32**, 1130–1138 (2011).
7. Nie, L. *et al.* In vivo volumetric photoacoustic molecular angiography and therapeutic monitoring with targeted plasmonic nanostars. *Small* **10**,1585–1593 (2014).
8. Huang, P. *et al.* Biodegradable gold nanovesicles with an ultrastrong plasmonic coupling effect for photoacoustic imaging and photothermal therapy. *Angew. Chem. Int. Ed. Engl.* **52**, 13958–13964 (2013).
9. Lin, J. *et al.* Photosensitizer-loaded gold vesicles with strong plasmonic coupling effect for imaging-guided photothermal/photodynamic therapy. *ACS Nano.* **7**, 5320–5329 (2013).
10. Wang, Y. H., Liao, A. H., Chen, J. H., Wang, C. R. & Li, P. C. A photoacoustic/ultrasound dual-modality contrast agent and its application to thermotherapy. *J. Biomed. Opt.* **17**, 045001 (2012).
11. Huang, X., Jain, P. K., El-Sayed, I. H. & El-Sayed, M. A. Gold nanoparticles: interesting optical properties and recent applications in cancer diagnostics and therapy. *Nanomedicine (Lond.)* **2**, 681–693 (2007).
12. Li, P. C. *et al.* In vivo photoacoustic molecular imaging with simultaneous multiple selective targeting using antibody-conjugated gold nanorods. *Opt. Express* **16**, 18605–18615 (2008).
13. Niidome, T. *et al.* Poly(ethylene glycol)-modified gold nanorods as a photothermal nanodevice for hyperthermia. *J. Biomater. Sci. Polym. Ed.* **20**, 1203–1215 (2009).
14. Pitt, W. G., Husseini, G. A. & Staples, B. J. Ultrasonic drug delivery–a general review. *Expert. Opin. Drug Deliv.* **1**, 37–56 (2004).
15. Anderson, C. R. *et al.* Ultrasound molecular imaging of tumor angiogenesis with an integrin targeted microbubble contrast agent. *Invest. Radiol.* **46**, 215–224 (2011).
16. Liao, A. H. *et al.* Evaluation of ^{18}F-labeled targeted perfluorocarbon-filled albumin microbubbles as a probe for microUS and microPET in tumor-bearing mice. *Ultrasonics* **53**, 320–327 (2012).
17. Lai, C. Y., Wu, C. H., Chen, C. C. & Li, P. C. Quantitative relations of acoustic inertial cavitation with sonoporation and cell viability. *Ultrasound Med. Biol.* **32**, 1931–1941 (2006).
18. Dijkmans, P. A. *et al.* Microbubbles and ultrasound: from diagnosis to therapy. *Eur. J. Echocardiogr.* **5**, 245–256 (2004).
19. Hutcheson, J. D., Schlicher, R. K., Hicks, H. K. & Prausnitz, M. R. Saving cells from ultrasound-induced apoptosis: quantification of cell death and uptake following sonication and effects of targeted calcium chelation. *Ultrasound Med. Biol.* **36**, 1008–1021 (2010).
20. Chu, S. W. *et al.* Multimodal nonlinear spectral microscopy based on a femtosecond Cr:forsterite laser. *Opt. Lett.* **26**, 1909–1911 (2001).
21. Hu, K. W. *et al.* Efficient near-IR hyperthermia and intense nonlinear optical imaging contrast on the gold nanorod-in-shell nanostructures. *J. Am. Chem. Soc.* **131**, 14186–14187 (2009).
22. Jun, H. Y. *et al.* Visualization of tumor angiogenesis using MR imaging contrast agent Gd-DTPA-anti-VEGF receptor 2 antibody conjugate in a mouse tumor model. *Korean J Radiol.* **11**, 449–456 (2010).

Acknowledgments

This research was partially funded by the National Health Research Institutes under grant NHRI-EX102-10137EI and the Science Council of Taiwan under grant NSC 99-2221-E-002-046-MY3.

Author contributions

The experiments were designed and conducted by Y.W. S.C. measured dICD and the intracellular concentration of AuNRs. The contrast agent was designed by A.L. AuNRs were synthesized by Y.Y., C.L. and C.W. Nonlinear microscopes were constructed and calibrated by C.W. and T.L. P.W. conducted the animal experiments involving the nonlinear microscope. The manuscript was written by Y.W. and P.L. P.L. is the PI of the project under which the study was performed.

Additional information

Competing financial interests: The authors declare no competing financial interests.

How to cite this article: Wang, Y.-H. *et al.* Synergistic delivery of gold nanorods using multifunctional microbubbles for enhanced plasmonic photothermal therapy. *Sci. Rep.* **4**, 5685; DOI:10.1038/srep05685 (2014).